AD-A083 025 CINCINNATI UNIV OHIO DEPT OF PHYSICS F/G 9/1
THEORETICAL INVESTIGATION OF THE EFFECTS OF ATMOSPHERIC GRAVITY--ETC(U)
DEC 79 T TUAN F19628-78-C-0208
UNCLASSIFIED AFGL-TR-80-0007 NL

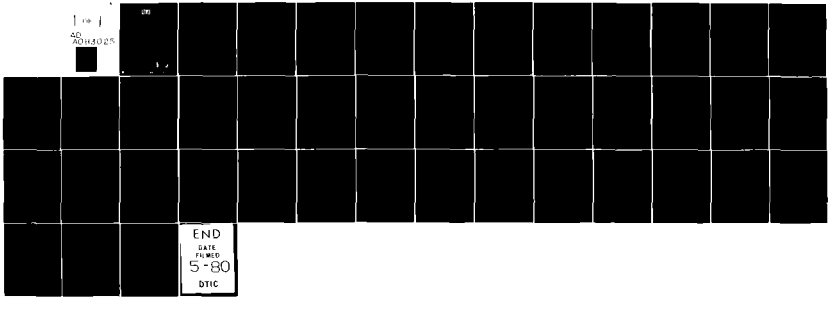

LEVEL II

AFGL-TR-80-0007

THEORETICAL INVESTIGATION OF THE EFFECTS OF ATMOSPHERIC GRAVITY WAVES ON THE NIGHTGLOW EMISSIONS OF THE ATMOSPHERE

Tai-Fu Tuan

University of Cincinnati
Physics Department
Cincinnati, Ohio 45221

Final Report
15 July 1978 - 30 November 1979

December 31, 1979

Approved for public release; distribution unlimited.

Unclassified

SECURITY CLASSIFICATION OF THIS PAGE (When Data Entered)

REPORT DOCUMENTATION PAGE

READ INSTRUCTIONS BEFORE COMPLETING FORM

1. REPORT NUMBER: AFGL-TR-80-0007
2. GOVT ACCESSION NO.: Final rept. 15 Jul 78 - 30 Nov 77
3. RECIPIENT'S CATALOG NUMBER

4. TITLE (and Subtitle): Theoretical Investigation of the Effects of Atmospheric Gravity Waves on the Hydroxyl Emissions of the Atmosphere
5. TYPE OF REPORT & PERIOD COVERED: Final 7/15/78 - 11/30/79
6. PERFORMING ORG. REPORT NUMBER

7. AUTHOR(s): Tai-Fu Tuan
8. CONTRACT OR GRANT NUMBER(s): F19628-78-C-0208

9. PERFORMING ORGANIZATION NAME AND ADDRESS: University of Cincinnati, Physics Department, Cincinnati, Ohio 45221
10. PROGRAM ELEMENT, PROJECT, TASK AREA & WORK UNIT NUMBERS: 61102F 2310G4AK

11. CONTROLLING OFFICE NAME AND ADDRESS: Air Force Geophysics Laboratory, Hanscom AFB, Massachusetts 01731, Monitor/Sam Silverman/OPR-1
12. REPORT DATE: Dec 1979
13. NUMBER OF PAGES: 40

14. MONITORING AGENCY NAME & ADDRESS (if different from Controlling Office)
15. SECURITY CLASS. (of this report): Unclassified
15a. DECLASSIFICATION/DOWNGRADING SCHEDULE

16. DISTRIBUTION STATEMENT (of this Report)

Approved for public release; distribution unlimited.

17. DISTRIBUTION STATEMENT (of the abstract entered in Block 20, if different from Report)

18. SUPPLEMENTARY NOTES

19. KEY WORDS (Continue on reverse side if necessary and identify by block number)

An analysis of the behaviour of hydroxyl emission under the influence of Atmospheric Gravity Waves.

20. ABSTRACT (Continue on reverse side if necessary and identify by block number)

The effect of gravity waves on OH emission is investigated using a gravity-wave model valid for an inhomogeneous atmosphere and computed as well as semi-empirical data for the "undisturbed" ozone and hydrogen profiles. The results show that (1) the magnitude of the response depends on the relative magnitudes and signatures of the vertical and horizontal

DD FORM 1 JAN 73 1473 EDITION OF 1 NOV 65 IS OBSOLETE S/N 0102-LF-014-6601

Unclassified

SECURITY CLASSIFICATION OF THIS PAGE (When Data Entered)

406 361

Block #20.

wave-induced diffusion. Since in some regions the horizontal velocity field of the gravity wave can increase much more rapidly with height than the vertical field, horizontal diffusion even when there is a relatively sharp layer gradient. (2) The structures in the OH profile produced by the gravity wave are in general but not always more pronounced below the intensity peak than above. The observed dark areas in OH emission can be produced by gravity waves with vertical wave length small compared with the half width of the intensity profile.

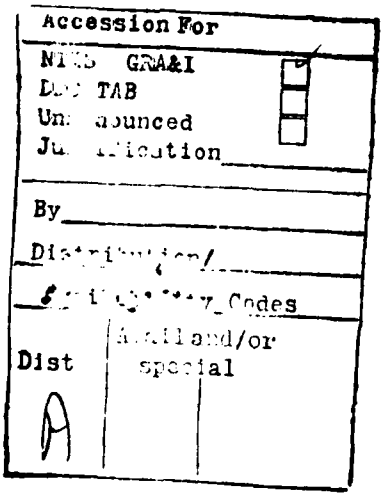

FINAL REPORT

Introduction

The association of intensity variation in atmospheric emissions with the presence of atmospheric waves has been made as far back as 1957 by Krassovsky (Krassovsky (1957)). Later, these effects have been observed and analyzed by a number of investigators [e.g. Okuda (1962), Silverman (1962), Barbier (1961, 1965), Weill and Christophe-Glaume (1967), Dachs, (1968), Andrews (1976), Dyson and Hopgood (1978)], for both the 6300 Å OI and the 5200 Å NI, The presence of gravity waves in OH emissions has been examined by Krassovksy (1972), Krassovsky and Shagaev (1974), Krassovsky et al (1975), Armstrong (1975), Krassovsky and Shagaev (1977), Moreels and Herse (1977), and Peterson (1979). Observations on the effect of gravity waves on $O_2(^1\Sigma)$ emissions have been made by Noxon (1978). Theoretical treatments for the effects of gravity waves on airglow have been made by Porter et al (1974) for 6300 Å OI and 5200 Å NI and Weinstock (1978) for $O_2(^1\Sigma)$ and OH emissions.

In general, the treatment of gravity wave effects on airglow require an analysis of the effects of gravity waves on the individual atmospheric constituents which produce the airglow through chemical reactions. There are two cases to be considered. The first is when the atmospheric constituents are minor components of the atmosphere. It is then usual to assume that the gravity waves are carried by the major atmospheric constituents and their effects on each of the minor constituents are analyzed with the assumption that the effects of the minor constituent on the gravity waves are negligible. The second case is when the atmospheric constituent producing the particular airglow emission is actually

itself the major constituent. In this case there is no longer a need to separately calculate the response of the constituent to the gravity waves. The problem of calculating airglow is then made much simpler provided a suitable gravity-wave model is chosen.

In calculating the effects of gravity waves on the oxygen red line and the nitrogen green line, it is necessary to first consider the effects of gravity waves on charged particles such as the electron, since it is primarily through dissociative recombination of these electrons with positive ions (O_2^+, NO^+) which produce these particular airglow emissions. The problem is further complicated by the presence of the magnetic field which puts additional constraints on the motion of the charged particles. Detailed knowledge of the response of the charged particles to the gravity wave including phase relations, magnitude of response etc. have been treated by Thome (1968), Testud and Francois (1971), Klostermeyer (1972a,b) and Porter and Tuan (1974). With the exception of Thome (1968), all the rest make use of gravity-wave models which include dissipation and also take into consideration the diffusion (ambipolar) of the charged particles. The calculations include: (1) the magnitude of the response which depends on the vertical gradient of the undisturbed ionospheric number density profile for the minor constituent, (2) the phase variation with height of the response relative to the gravity waves.
Here we should mention that it was Thome (1968) who first observed a 180° phase change in the response of the F-layer above and below the F-region peak and provided a suitable physical

explanation. Subsequent theoretical papers by Testud and Francois (1971), Klostermeyer (1971a,b) and Porter and Tuan (1974) have quantitatively confirmed the phase variation.

To calculate the effects of gravity waves on OH emission it is necessary to know the effect of gravity waves on neutral minor atmospheric constituents such as H and O_3. The effects of gravity waves on neutral atmospheric constituents have been considered by Dudis and Reber (1976) who use the Hines isothermal gravity-wave model and neglect wave-induced diffusion to obtain simple analytic phase relationships between the response of the atmospheric constituent and the gravity wave. The method is justifiable for lower atmospheres where dissapation is not crucial and for free gravity wave modes with low horizontal phase velocity (less than 100 m/sec.). Chiu and Ching (1978) have considered the effect of gravity waves on minor constituents with a layered Structure. Like Dudis and Reber (1976) they have used the Hines (1960) analytic model for the gravity wave and obtained similar relationships in terms of well-known atmospheric parameters such as the scale height and the ratio of specific heats, etc. While their conclusions are essentially similar to those mentioned in the previous paragraph, they also specifically point out that the response for the bottom side is always greater than the top side. This last result is only strictly true for a Hines' gravity wave model in which the rate of increase of the horizontal and vertical velocity components with height are always the same.

In this paper we wish to consider the effect of gravity

waves on OH emissions using a gravity-wave model [Tuan (1976)] which satisfies the rigid surface boundary condition at the ground level and can provide for guided as well as free modes. The undisturbed hydrogen and ozone profiles are taken from Good (1976) and Keneshea and Zimmerman (private communication). We will consider the effect of gravity waves on the OH emission profile for different horizontal phase velocities. It will be shown that for sufficiently low horizontal phase velocity (~ 33 m/sec.) the gravity wave can produce structures in the OH emission profile and that the structures tend to but need not always be more pronounced on the bottom side. These structures reveal the presence of dark areas usually observed below the peak intensity which appear to correspond to the "holes" observed by Peterson (1978). We will consider the "phase" relationship between the response of H and O_3 and the gravity wave. In this case, just as for the case of the ionosphere, the "phase" varies continually from the bottom side to the top side. Here, we use the word "phase" only in a very approximate sense, since neither our gravity-wave model nor the response of the atmospheric constituents have a simple periodic spatial variation.

For the case of large horizontal phase velocities (say, > 160 m/sec.), the vertical "wave length" is then too large compared with the thickness of the ozone layer to produce any significant spatial structures. However, there will, of course, be significant temporal variation in the total columnar intensity which can be observed by a ground-based photometer.

Theoretical Formulation

We shall assume that the primary mechanism for the production of OH emissions is given by the reaction

$$H + O_3 \xrightarrow{k(v)} OH(v) + O_2 \qquad (1)$$

The OH intensity profile I (photon/km^{3}sec) is then given by:

$$I = \mathcal{Z} \sum k(v) \quad [H] \quad [O_3] \qquad (2)$$

where $\mathcal{Z}$ is the efficiency of photon emission per OH molecule formed and k(v) is the rate coefficient for equation (1). It is possible to show that in regions between 80 km and 100 km [Earl Good (1976), Zimmerman (private communication)] chemical equilibrium is a good assumption for the production and loss of ozone. Thus, from equation (2), all we need is to determine the effect of gravity waves on the hydrogen and ozone profiles. Since both are obviously very much minor atmospheric constituents, corresponding to the first case mentioned in the Introduction, we shall assume that the gravity wave is being carried by the major constituents and consider its effect on H and O_3 separately. We shall also, for the present paper, make use of the linearized (perturbation) approach and will specify other approximations as they appear. The continuity equation, momentum conservation equation for any given minor

atmospheric [illegible] equations:

$$\frac{\partial N}{\partial t} = q - L - \operatorname{div}(N\vec{v}) \tag{3}$$

$$mN\frac{D\vec{v}}{Dt} + mN\nu(\vec{v} - \Delta\vec{v}_g) = -\left[\nabla\vec{p} - mN\vec{g}\right] \tag{4}$$

where N = concentration of the minor component

$\vec{v}$ = velocity field

m = molecular mass of the component

ν = collision frequency between the component and the major atmospheric constituents

p = partial pressure of the minor component

$\Delta\vec{v}_g$ = gravity-wave velocity field given by the gravity-wave model

q = production rate

L = loss rate

Even with the assumption of a model for $\Delta\vec{v}_g$, equations (3) and (4) are not closed. An additional condition for the equation of state is needed to close the system of equations. However, in general we may need different equations of state for the perturbed and the unperturbed atmospheric constituent.

For instance, if the perturbation is an oscillation, we may require the adiabatic condition which, however, cannot be validly applied to the unperturbed atmosphere. Thus, we will leave the equations open and close them with one or more appropriate equations of state as the need arises. We will assume

$$
\begin{aligned}
N &= N_0 + \Delta N \\
q &= q_0 + \Delta q \\
L &= L_0 + \Delta L \\
p &= p_0 + \Delta p \\
\vec{V} &= \vec{V_d} + \vec{\Delta V}
\end{aligned}
\tag{5}
$$

where N_0, q_0, L_0, and p_0 are the background concentration, etc. of the minor constituent undisturbed by the gravity wave. $\vec{V_d}$ is the drift velocity of the minor constituent through the background atmosphere and is always strong whenever there is a sharp concentration gradient. We shall assume that these dependent variables are independent of time and are functions of z only (horizontal stratification). ΔN, Δq, ΔL, Δp, and $\vec{\Delta V}$ are the perturbed dependent variables produced by the gravity wave. We shall also neglect variation in collision frequency.

Substituting equation (5) into (3) and (4) we obtain the

following zeroth order equations

$$0 = q_0 - L_0 - \frac{\partial(N_0 V_z)}{\partial z} \tag{6}$$

$$m N_0 \nu_c V_d = -\frac{\partial p_0}{\partial z} - m N_0 g \tag{7}$$

It is possible to show that for ozone the divergence term in equation (6) is not important for height ranges between 80 km and 100 km [Zimmerman (private communication)]. However, the drift velocity term for equation (7) cannot be neglected.

The first order equations are given by:

$$\frac{\partial(\Delta N)}{\partial t} = \Delta q - \Delta L - \mathrm{div}(N_0 \overrightarrow{\Delta V}) \tag{5}$$

$$m N_0 \frac{\partial(\Delta u)}{\partial t} + m N_0 \nu(\Delta u - \Delta u_g) = -\frac{\partial(\Delta p)}{\partial x} \tag{6}$$

$$m N_0 \frac{\partial(\Delta w)}{\partial t} + m N_0 \nu(\Delta w - \Delta w_g) + m \Delta N \nu V_d = -\frac{\partial(\Delta p)}{\partial z} - m \Delta N g \tag{7}$$

where $\overrightarrow{\Delta V} = (\Delta u, \Delta w)$, $\overrightarrow{\Delta V_g} = (\Delta u_g, \Delta w_g)$

With the assumption of horizontal stratification, we seek solutions of the form:

$$f(z)\, e^{i(\omega t - k_x x)}$$

where ω is the gravity-wave frequency and k_x the horizontal wave vector. The equations become,

$$i\omega \Delta N = \Delta q - \Delta L + i k_x N_o \Delta u - \frac{\partial (N_o \Delta W)}{\partial z} \tag{8}$$

$$\Delta u = \Delta u_g + \frac{i k_x}{m N_o \nu} \Delta p - i\left(\frac{\omega}{\nu}\right) \Delta u \tag{9}$$

$$\Delta W = \Delta W_g - i\left(\frac{\omega}{\nu}\right) \Delta W - \frac{g}{N_o \nu} \Delta N - \frac{1}{m N_o \nu} \frac{\partial (\Delta p)}{\partial z} - V_d \left(\frac{\Delta N}{N_o}\right) \tag{10}$$

We shall now consider the right-hand side of equations (9) and (10). The collision frequency ν at 100 km is of the order of 2×10^3 sec^{-1}, while the gravity wave angular frequency for a 2 hour period is of the order of 8.7×10^{-4} sec^{-1}. Hence,

$$\frac{\omega}{\nu_o} \sim 4 \times 10^{-7} \tag{11}$$

We can immediately neglect the two velocity terms. For the term involving g, we have

$$\frac{g}{\nu_c}\left(\frac{\Delta N}{N_c}\right) \sim 4.5 \times 10^{-3} \left(\frac{\Delta N}{N_c}\right) \text{ m sec}^{-1} \tag{12}$$

Now $\left|\frac{\Delta N}{N_0}\right| < 1$, and ΔW_j is of the order of 0.5 m. sec.$^{-1}$ so we can neglect this term.

The pressure term in equation (9) may be written as

$$\frac{k_x}{N_0 D}(\Delta p) \sim k_x D\left(\frac{\Delta p}{p_0}\right) \qquad (13)$$

where D is the diffusion coefficient of the gas.

The drift velocity term is given by

$$-v_d\left(\frac{\Delta N}{N_0}\right) \sim \frac{D}{N_0}\frac{\partial N_0}{\partial z}\left(\frac{\Delta N}{N_0}\right) \qquad (14)$$

In general, the diffusion coefficient D is of the order of 200 m^{2}sec^{-1} at 100 km. For the bottom side of ozone $\frac{1}{N_0}\frac{\partial N_0}{\partial z} \sim$ 0.4 x 10^{-3} m.$^{-1}$ Hence $v_d \sim 8 \times 10^{-2}$ m.sec^{-1}.
Since $\left|\frac{\Delta N}{N_0}\right| < 1$, we may neglect this term in comparison with ΔW_j. The pressure term in equation (9) may be written as

$$\frac{k_x}{N_0 D}(\Delta p) \sim k_x D\left(\frac{\Delta p}{p_0}\right) \qquad (15)$$

Since maximum $k_x \sim 6 \times 10^{-5}$ m.$^{-1}$ and $\left|\frac{\Delta p}{p_0}\right| < 1$

$k_x D\left(\frac{\Delta p}{p_0}\right) \sim .012\left(\frac{\Delta p}{p_0}\right)$ m.sec^{-1}, which is again negligible.

The term $\frac{1}{m N_0 \nu_c} \frac{\partial(\Delta p)}{\partial z}$ can be approximately written as

$$\frac{1}{m N_0 \nu_c} \frac{\partial(\Delta p)}{\partial z} \sim i k_z D \left(\frac{\Delta p}{p_0}\right) \tag{16}$$

where we assume that to a rough approximation, Δp can be approximated by a sinusoidal wave with vertical wave-vector k_z. The maximum k_z we consider corresponding to a horizontal phase velocity of about 33 m/sec, is of the order of $k_z \sim 1.3 \times 10^{-3}$ m.$^{-1}$. This means that $k_z D\left(\frac{\Delta p}{p_0}\right) \sim 0.26 \left(\frac{\Delta p}{p_0}\right)$ m.sec.$^{-1}$, which is again very much less than the typical value of Δw of some m.sec.$^{-1}$. Thus, for all horizontal phase velocity of interest, we may assume that equations (9) and (10) reduce to

$$\Delta u = \Delta u_g \tag{17}$$

$$\Delta w = \Delta w_g \tag{18}$$

Substituting equations (17) and (18) into equation (8) and assuming that $\Delta q \sim \Delta L$ we obtain:

$$\Delta N = \frac{N_0 k_x}{\omega} \Delta u_g + \frac{i}{\omega} \frac{\partial(N_0 \Delta w_g)}{\partial z} \tag{19}$$

Thus, given any gravity-wave model, we can calculate ΔN from equation (19).

Gravity-wave model

The gravity-wave model we use [Tuan (1976)] satisfies the rigid surface boundary condition at the ground level and propagates in an atmosphere in which the variations in temperature, mean molecular mass, acceleration due to gravity and ratio of specific heats are all taken into account using the 1972 COSPAR model wherever feasible. The model also allows for the propagation of discrete as well as for the continuous or free modes. Since we are only concerned with altitudes below 110 km, dissipation due to thermal conduction, viscosity and ion drag may be neglected. In the complex notation, Δw_g is actually pure imaginary, so ΔN is actually real in equation (19). In general, the boundary condition at the ground ensures that the dependent variables (i.e., Δw_g or Δu_g), which are functions of z only, are either pure real or pure imaginary. Since we use a complex time dependence [exp ($i\omega t$)], this means that there is a stationary wave along the vertical direction in contrast to the travelling wave along the horizontal direction, an expected result for a rigid surface boundary condition.

The model we use [Tuan (1976)] actually only calculates the pressure variation given by

$$\psi = \frac{\omega \Delta p_g}{\sqrt{\rho_0}} \tag{20}$$

where ρ_0 is the background density and Δp_g is the pressure

variation of the gravity wave. The velocity field may be obtained from the pressure field through the hydrodynamic equations and the results are given by

$$\Delta u_g = \frac{k_x}{\omega^2 \sqrt{\rho_0}} \psi$$

$$\Delta W_g = \frac{-i}{\sqrt{\rho_0}\, \omega_b^2} \left[\frac{\partial \psi}{\partial z} - \lambda(z) \psi \right] \tag{21}$$

where $\lambda(z) = \left(\frac{\gamma g}{2c^2} + \frac{c'}{c} - \frac{g}{c^2} \right)$

In equation (21), since ψ obeys the boundary condition [Tuan (1976)]

$$\left. \frac{\partial \psi}{\partial z} \right|_{z=0} = \lambda(0) \psi \Big|_{z=0} \tag{22}$$

The vertical velocity field obeys the usual well-known boundary condition of $\Delta W(0) = 0$.

Figs (1) and (2) show the vertical and horizontal velocity fields ΔW and ΔU as functions of z, the altitude, for horizontal phase velocities of 302 and 33 m/sec, respectively. For both the vertical and horizontal velocity fields there are nodes along the vertical direction. This means that there are adjacent layers where the particles move in opposing directions. The approximate vertical wave lengths are of the order of 150 - 200 km and 8 km, respectively. Since the total half

width of, for instance, the hydrogen number density profile is of the order of 10 km, spatial structures are expected only for the gravity wave with a horizontal phase velocity of 33 m/sec^{-1} (or less). Here, we should mention that the 302 $m/sec.^{-1}$ wave is very close to the guided Lamb mode so that "vertical wave length" is meaningless below 100 km altitude, where the length scale in the atmospheric structure is less than the wave length and the Hines (1960) model is no longer valid. At least for this altitude range (80 - 105 km) the horizontal velocity field increases with height far more rapidly than the vertical velocity field. In Fig. (1) our gravity-wave model shows a maximum horizontal velocity of 84 $m/sec.^{-1}$ at 91 km. This is consistent with Peterson's estimation (1979) of 71 $m/sec.^{-1}$ at an assumed 90 km altitude from an observed OH emission.

Results

For the unperturbed hydrogen and ozone number density profiles, we use the semi-empirical data of Good (1976) and Keneshea and Zimmerman (private communication). In Figs. (3) and (4) we show the "unperturbed" variations in the ozone and hydrogen number density as a function of altitude. The Zimmerman data is used throughout for both Figures. We see that the hydrogen concentration has a peak at between 84 to 85 km while the ozone has a local peal at about 86 km.

The concentration gradient, at least for the hydrogen (Fig. 5) curve, is steeper below the peak than above the peak.

Fig. (5) shows variations in ozone $\Delta N(O_3)$, hydrogen $\Delta N(H)$ and total ΔN_T number densities when a gravity wave with a horizontal phase velocity of 302 $m.sec^{-1}$ and a two-hour period passes by. In Figs. (5) to (10) (inclusive) the number density variations ΔN are all computed from equation (19). For Figs. (5) to (9) (inclusive) we have used Zimmerman's data for the unperturbed concentration profile N_o. For Fig.(10) we have used Earl Good's (1976) data for the unperturbed profile. The two terms on the right-hand side of equation (19) represent the individual contributions from the horizontal and vertical diffusion to ΔN . For both the minor constituents [5(a) and 5(b)] the vertical diffusion is predominant below the peaks. Since the horizontal diffusion has the same sign (negative) as the vertical, there is significant reinforcement. The vertical diffusion tends to dominate below the peak because of the relatively steep vertical concentration gradient. At the same time, the horizontal velocity field below the peaks is not yet sufficiently greater than the vertical that horizontal diffusion can effectively compete with the vertical diffusion. We might mention that because the horizontal and vertical diffusion reinforce each other for both minor constituents, the response is significantly

greater below peak for V_{phx} = 302 m.sec^{-1} than for other gravity waves with lower horizontal phase velocities. For ΔN_T there is no sharp vertical concentration gradient (no peaks) for the unperturbed total atmospheric concentration and the horizontal diffusion dominates.

Unlike the minor constituents, there is considerable cancellation between vertical and horizontal diffusion in ΔN_T, which also accounts in part for the very large response (i.e., large ratios for $\Delta N(O_3)/\Delta N_T$ and $\Delta N(H)/\Delta N_T$ as compared with other gravity waves. Above the hydrogen and ozone peaks vertical domination continues for ozone but for hydrogen, which has a less steep vertical gradient, horizontal diffusion eventually becomes dominant. The ΔN_T of course continues to have large cancellation with a horizontal domination.

Fig. (6) shows $\Delta N(O_3)$, $\Delta N(H)$ and ΔN_T for a gravity wave with a horizontal phase velocity of 78 m.sec.$^{-1}$ Below the peaks, we again have high vertical domination for the minor constituents with a horizontal domination at lower altitudes for ΔN_T. Here cancellation occurs to a much less extent than for the previous case. Above the peaks, horizontal domination eventually takes over for both ozone and hydrogen. In both Fig. (6a) and (6b), one can begin to see a phase change in the response of the minor constituent relative to ΔN_T. Below the peaks the response is out of phase, but above the peaks they appear

greater below peak for V_{phx} = 302 m.sec^{-1} than for other gravity waves with lower horizontal phase velocities. For ΔN_T there is no sharp vertical concentration gradient (no peaks) for the unperturbed total atmospheric concentration and the horizontal diffusion dominates.

Unlike the minor constituents, there is considerable cancellation between vertical and horizontal diffusion in ΔN_T, which also accounts in part for the very large response (i.e., large ratios for $\Delta N(O_3)/\Delta N_T$ and $\Delta N(H)/\Delta N_T$ as compared with other gravity waves. Above the hydrogen and ozone peaks vertical domination continues for ozone but for hydrogen, which has a less steep vertical gradient, horizontal diffusion eventually becomes dominant. The ΔN_T of course continues to have large cancellation with a horizontal domination.

Fig. (6) shows $\Delta N(O_3)$, $\Delta N(H)$ and ΔN_T for a gravity wave with a horizontal phase velocity of 78 m.sec.$^{-1}$ Below the peaks, we again have high vertical domination for the minor constituents with a horizontal domination at lower altitudes for ΔN_T. Here cancellation occurs to a much less extent than for the previous case. Above the peaks, horizontal domination eventually takes over for both ozone and hydrogen. In both Fig. (6a) and (6b), one can begin to see a phase change in the response of the minor constituent relative to ΔN_T. Below the peaks the response is out of phase, but above the peaks they appear

to get in phase.

In Fig. (7), the vertical diffusion again dominates below the peaks for the minor constituents. For ΔN_T there is horizontal domination only at lower altitudes. Above the peaks, horizontal domination and some cancellation occur for both hydrogen and ozone. Once again, one can see that the response of the minor constituents is out of phase with the major constituents below the peaks but gets in phase above the peaks.

In Fig. (8) and (9) we show separately the response of $\Delta N(O_3)$ and $\Delta N(H)$ as compared with ΔN_T. With a vertical wave length approximately in the range of 8 - 9 km one can see rather easily the response which is about 180° out of phase below say 87 km but gets almost completely in phase above 90 km. The gravity wave used here has a horizontal phase velocity of 33 $m.sec.^{-1}$ and we have used both Zimmerman's data (Fig. 8 and 9) and Earl Good's data (Fig. 10) to show up any significant difference in the response of the minor constituents. All in all there is relatively little qualitative difference in the basic features. For both sets of data, there is either vertical domination or large cancellation (for hydrogen and Earl Good's data) below the peaks. Above the peaks, there is either horizontal domination and large cancellation (for Earl Good's data) or alternating vertical and horizontal domination (for Zimmerman's data).

Finally, we use equation (2) to calculate the total hydrogen intensity profile for a gravity wave with V_{phx} = 33 m.sec.$^{-1}$ For this case, as already mentioned, the vertical wave length is less than the half width of the unperturbed OH profile and one would expect structures to occur. Fig. (11) shows the OH intensity profile, using Zimmerman's unperturbed data. Fig. (12) shows the profile using Earl Good's (1976) data. We see immediately for both curves a double layered structure below the peak and a suggestion of some kind of structure above the peak. It is obvious that the structure below the peak is far more pronounced than above the peak in agreement with the analysis of Chiu and Ching (1978) in which the Hines (1960) gravity-wave model was used. The "valley" immediately below the peak can easily correspond to the "dark areas" observed by Peterson (1978). While we have found that it is sometimes possible (depending on the phase of the gravity wave) to observe structure above the peak OH intensity rather than below, it is more likely to find highly pronounced structures below peak intensity.

In our computing procedure, the only real difficulty comes from numerical differentiation. In obtaining ΔN in equation (19), we essentially have to differentiate the function ψ given by equation (20) twice, once through equation (21) and once through equation (19). Various smoothing procedures have been adopted but were found to

be unreliable because they tend to alter the phase of the final ΔN. In the end, we have decided to plot the curves in Fig. 5-10 without any smoothing. Much of the structures in ΔN_T in Fig. 5(a) and Fig. 5(b) is caused by small irregularities in the original function ψ which become greatly exaggerated when it is twice differentiated. These irregularities become much less influential when ψ itself has a much smaller vertical wave length, as can be seen in Fig. (8), (9), and (10) in which ΔN_T are essentially smooth oscillating curves.

Conclusion

The principal features of the present investigation may be summarized as follows: (1) We have found that the variations ΔN in number densities of hydrogen and ozone produced by gravity waves can be attributed primarily to wave induced vertical diffusion below the layer peak and a mixture of horizontal and vertical diffusion above the peak. For the most part, the contribution of this vertical diffusion is negative creating a decrease in the number density from the unperturbed profile. The vertical diffusion dominance can be in part attributed to the relatively steep vertical gradient for the minor constituents. The increase in importance of the horizontal diffusion above the peak can be in part attributed to the good deal more rapid increase with height in the horizontal velocity field as

compared with the vertical field and in part to the less steep vertical concentration gradient above the peak.

(2) The phase of the response relative to the gravity wave varies continually with altitude and is 180° out of phase well below the peak but comes in phase well above the peak, in agreement with the original results of Thome (1968).

(3) On the whole (but not always) the structures produced by the OH emission profile are more pronounced below the peaks of hydrogen and ozone than above and pronounced dark areas can occur immediately below the peak OH intensity.

Acknowledgments

We like to express our appreciation to Dr. S. P. Zimmerman for making some of his data and theoretical calculations on the hydrogen and ozone profiles available to us and to Dr. A. T. Stair for some helpful discussions. The work is supported in part by Air Force Grant AF 19628-78C-0208.

References

(1) Andrews, M.K., Wavelike irregularities in the mid-latitude 6300 Å airglow, Planet. Space Sci. 24, 521-527, (1976).

(2) Armstrong, E.B., The influence of a gravity wave on the airglow hydroxyl rotational temperature at night, J. Atmos. Terr. Phys. 37, 1585-1591 (1975).

(3) Barbier, D., Observation photometrique d'une perturbation de la haute atmosphere, Astrophys. Norv. 9, 55-59 (1964).

(4) Barbier, D., Deux phenomenes particuliers presentee par le raie rouge de la lumiere du ciel nocturne, Ann. Geophys. 21, 228-234 (1965).

(5) Chiu, Y.T. and B.K. Ching, The response of atmospheric and lower ionospheric layer structures to gravity waves, Geophys. Res. Lett. 5, 539-542 (1978).

(6) Dachs, J. Die Helligkeiten der nachtlichen Luftleuchten wahrend der Sommerflechen Minimum nach Messungen in Sudwestafrika. Beitr. Phys. Atmos. 41, 184-215 (1968).

(7) Dudis, J.J. and C.A. Reber, Composition effects in thermospheric gravity waves, Geophys. Res. Lett. 3, 727-730 (1976).

(8) Dyson, P.L. and P. A. Hopgood, Fluctuations in mid-latitude 6300 Å airglow and their relationship to F-region irregularities, Planet. Space Sci. 26, 161-169 (1978).

(9) Good, R.E., Determination of atomic oxygen density from frocet borne measurement of hydroxyl airglow, Planet. Sci. 24, 389-395 (1976).

(10) Hines, C.O., Internal atmospheric gravity waves at ionospheric heights, Can. J. Phys. 38, 1441-1481 (1960).

(11) Klostermeyer, J., Numerical calculation of gravity-wave propagation in a realistic thermosphere, J. Atmos. Terr. Phys. 34, 765-774 (1972a).

(12) Klostermeyer, J., Comparison between observed and numerically calculated atmospheric gravity waves in the F-region, J. Atmos. Terr. Phys. 34, 1393-1401 (1972b).

(13) Krassovsky, V.I., Nature of the intensity variations of the terrestrial atmosphere emission, Memoires de la Societe Royale des Sciences de Liege, 18, 58-67, (1957).

(14) Krassovsky, V.I., Infrasonic variation of OH emission in the upper atmosphere, Ann. Geophys. 28, 739-746 (1972).

(15) Krassovsky, V.I. and M.V. Shagaev, Optical method of recording accoustic or gravity waves in the upper atmosphere, J. Atm. Terr. Phys. 36, 373-375 (1974).

(16) Krassovsky, V.I., B.P. Potapov, A.I. Seminov, M.V. Shagaev, N.N. Shefov, V.G. Sobolev and T.I. Toroshuledze, Internal gravity waves near the mesopause and the hydroxyl emission, Ann. Geophys. 33, 347-356 (1977).

(17) Krassovsky, V.I. and M.V. Shagaev, On the nature of internal gravity waves observed from hydroxyl emission, Planet. Space Sci. 25, 200-201 (1977).

(18) Moreels, G. and M. Herse, Photographic evidence of waves around the 85 km level, Planet. Space Sci. 25, 265-271 (1977).

(19) Noxon, J.F., Effect of internal gravity waves upon night airglow temperatures, G.G.L. 5, 25-27 (1978).

(20) Okuda, M., A study of excitation process in nightglow, Sci. Rep. Tohuko Univ. Ser. 5, 14, 9-26 (1962).

(21) Peterson, A.W., Visible OH airglow events--a problem area for the spectroscopist, Technical Digest, Topical Meeting on Atmospheric Spectroscopy, (Aug. 30-Sept. 1) WA2-1 (1978).

(22) Peterson, A.W., Airglow events visible to the naked eye, Applied Optics 18, 3390-3393 (1979).

(23) Porter, H.S., S.M. Silverman and T.F. Tuan, On the behavior of airglow under the influence of gravity waves, J. Geophys. Res. 79, 3827-3833 (1974).

(24) Porter, H.S. and T.F. Tuan, On the behavior of the F-layer under the influence of gravity waves, J. Atmos. Terr. Phys. 36, 135-157 (1974).

(25) Silverman, S.M., Unusual fluctuations of 5577 Å OI airglow emission intensity on Oct. 28-29, 1961, Nature 195, 481-482 (1962).

(26) Testud, J. and P. Francois, Importance of diffusion processes in the interaction between neutral waves and ionization, J. Atm. Terr. Phys. 33, 765-774 (1971).

(27) Thome, G.D., Long-period waves generated in the polar ionosphere during the onset of magnetic storms, J. Geophys. Res. 73, 6319-6336 (1968).

(28) Tuan, F.T., Research in gravity waves and airglow phenomena, Report, AFGL-TR-76-0296 (1976).

(29) Weill, G. and J. Christophe-Glaume, L'excitation du doublet interdit ^4S-^2D de l'azote observee dans la luminescence notcurne au cours d'une perturbation ionospherique itinerante, C.R. Acad. Sci. 264, 1286-1289 (1967).

(30) Weinstock, J., Theory of the interaction of gravity waves with $O_2(^1\Sigma)$ airglow, J. Geophys. Res. 83, 5175-5185 (1978).

Figure Captions

Fig. 1 Gravity wave model for a horizontal phase velocity of 302 m.sec.$^{-1}$ ΔW and ΔU are the vertical and horizontal velocity fields respectively.

Fig. 2 Gravity wave model for a horizontal phase velocity of 33 m.sec^{-1}. ΔW and ΔU are the vertical and horizontal velocity fields.

Fig. 3 Unperturbed ozone number density profile.

Fig. 4 Unperturbed hydrogen number density profile.

Fig. 5(a) A comparison of the variations in ozone number density ΔN (O_3) and total number density ΔN_T produced by a gravity wave with a horizontal phase velocity of 302 m.sec.$^{-1}$

Fig. 5(b) A comparison of the variations in hydrogen number density ΔN (H) and total number density ΔN_T produced by a gravity wave with a horizontal phase velocity of 302 m.sec.$^{-1}$

Fig. 6(a) A comparison of the variations in ozone ΔN (O_3) and total number density ΔN_T produced by a gravity wave with a horizontal phase velocity of 78 m.sec.$^{-1}$

Fig. 6(b) A comparison of the variations for hydrogen ΔN (H) and total number density ΔN_T produced by a gravity wave with a horizontal phase velocity of 78 m.sec.$^{-1}$

Fig. 7(a) A comparison of the variations for ozone ΔN (O_3) and total number density ΔN_T produced by a gravity wave with a horizontal phase velocity of 60 m.sec.$^{-1}$ The two curves are out of phase below 90 km. but begin to get in phase above this height.

Fig. 7(b) A comparison of the variations for hydrogen ΔN (H) and total number density ΔN_T produced by a

gravity wave with a horizontal phase velocity of 60 m.sec.$^{-1}$ Again, the two curves are out of phase below 86 km. and begin to get in phase above this height.

Fig. 8 A comparison of the variations for ozone $\Delta N\ (O_3)$ and total number density ΔN_T produced by a gravity wave with a horizontal phase velocity of 33 m.sec.$^{-1}$ For this case, the two curves are obviously out of phase below 90 km. and are quite evidently in phase at high altitudes.

Fig. 9 A comparison of the variations in hydrogen $\Delta N\ (H)$ and total number density ΔN_T produced by a gravity wave with a horizontal phase velocity of 33 m.sec.$^{-1}$ Again, the two curves are clearly out of phase at low altitudes and are perfectly in phase above 90 km.

Fig.10(a) The same curves as those in Fig. 8 are plotted using Earl Good's data for unperturbed ozone profile.

Fig.10(b) The same curves as those in Fig. 9 are plotted using again Earl Good's data for unperturbed hydrogen profile.

Fig. 11 OH intensity profile in the presence of a gravity wave with a horizontal phase velocity of 33 m.sec.$^{-1}$ Zimmerman's data are used for the unperturbed ozone and hydrogen profiles.

Fig. 12 OH intensity profile in the presence of a gravity wave with a horizontal phase velocity of 33 m.sec.$^{-1}$ Earl Good's data are used for the unperturbed ozone and hydrogen profiles.

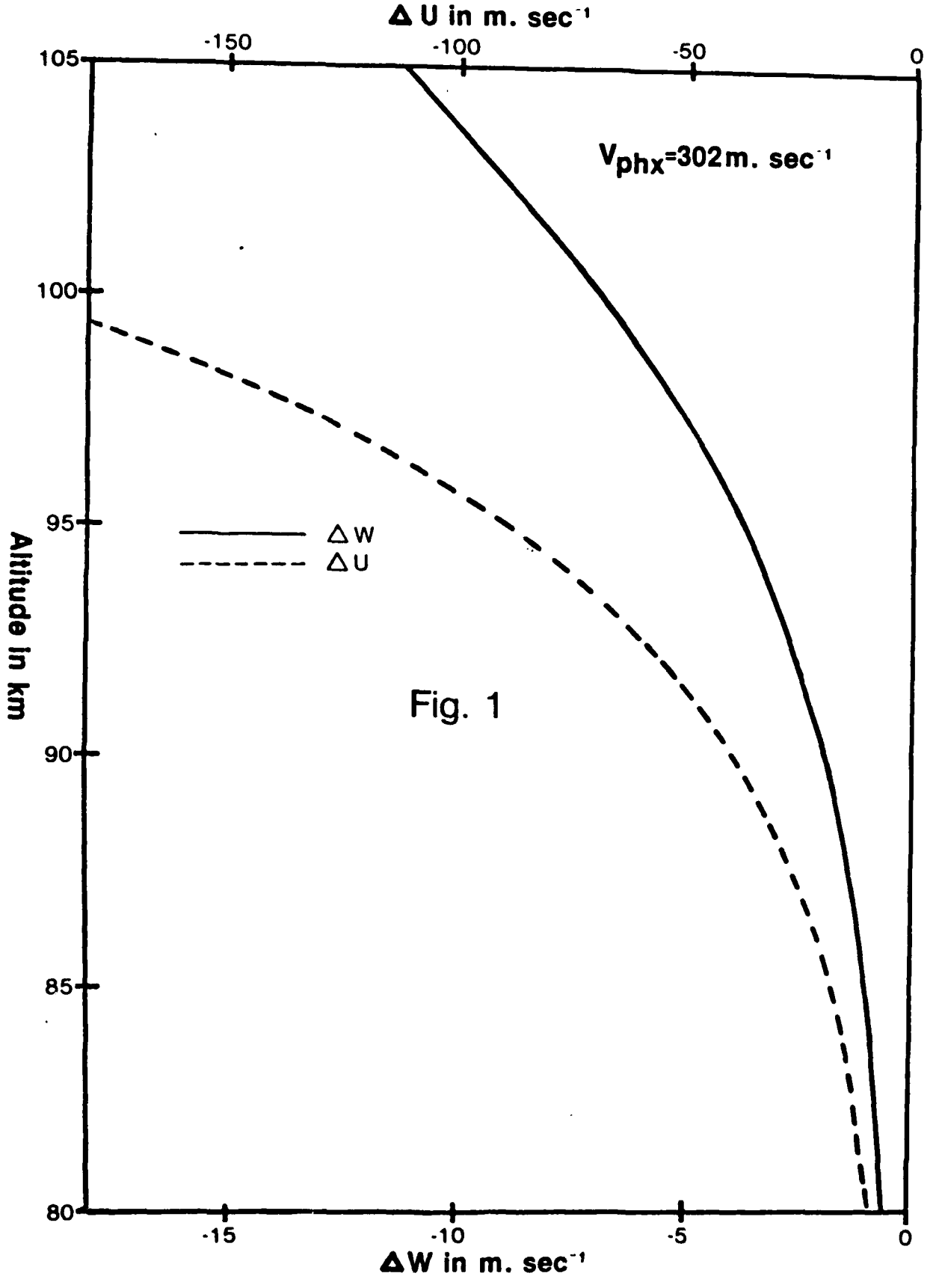
Δ U in m. sec⁻¹
-150
-100
-50
0
105
100
95
90
85
80
V_{phx}=302m. sec⁻¹
Δ W
Δ U
Altitude in km
-15
-10
-5
0
ΔW in m. sec⁻¹

Fig. 1

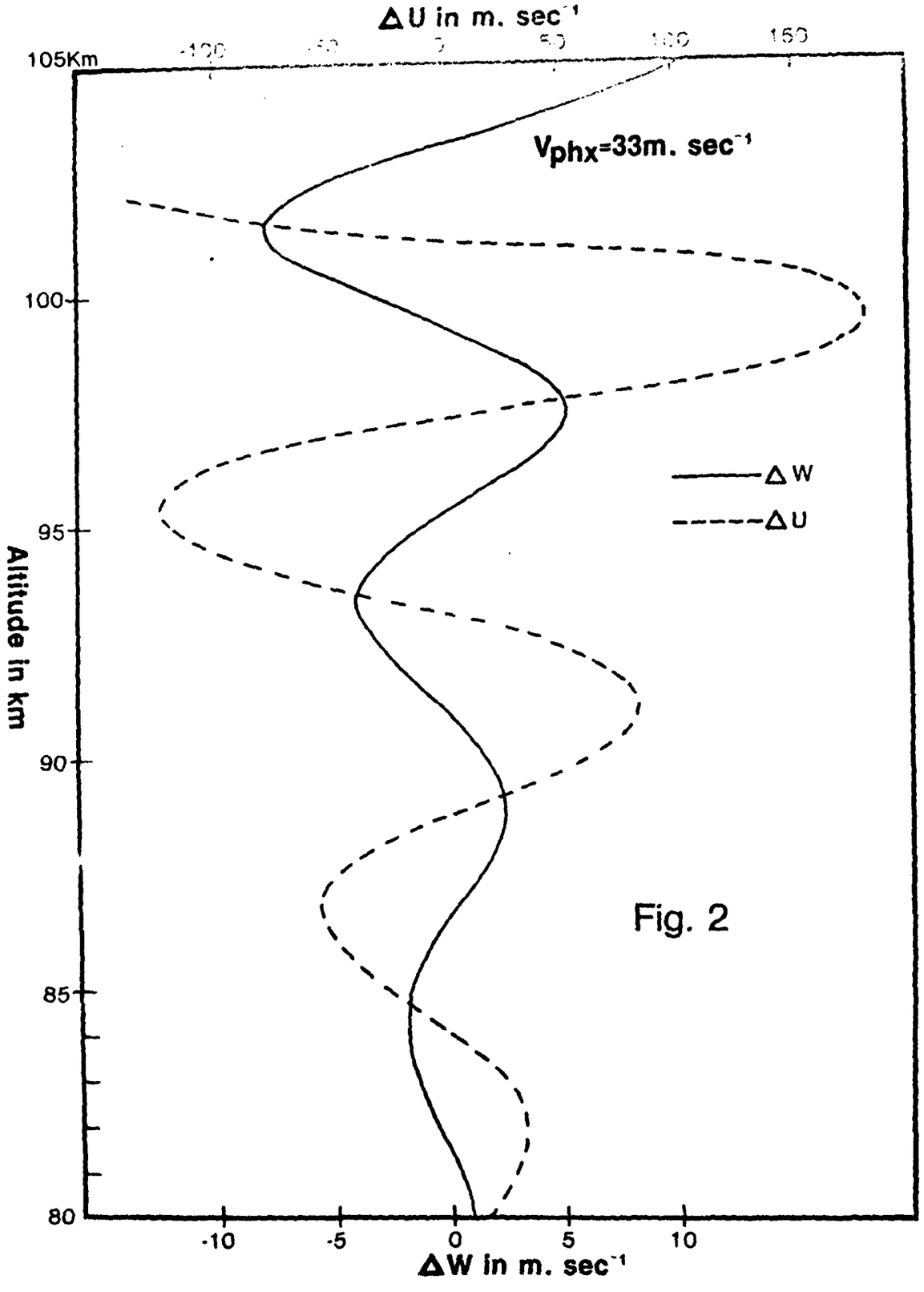
ΔU in m. sec⁻¹
105Km
100
95
90
85
80
Vphx=33m. sec⁻¹
ΔW
ΔU
Altitude in km
-10
-5
0
5
10
ΔW in m. sec⁻¹

Fig. 2

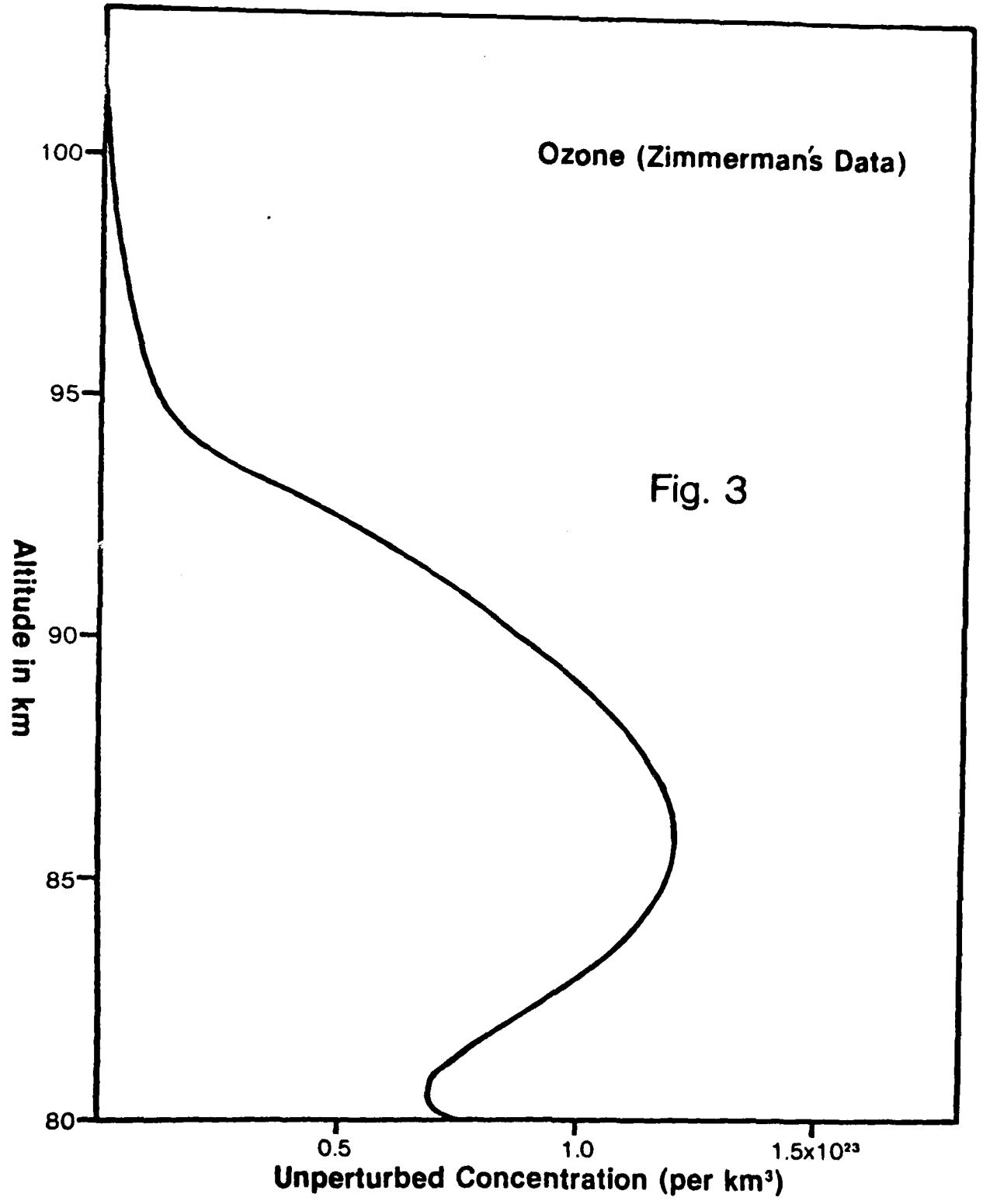
Ozone (Zimmerman's Data)
100
95
90
85
80
Altitude in km
0.5
1.0
1.5x10²³
Unperturbed Concentration (per km³)

Fig. 3

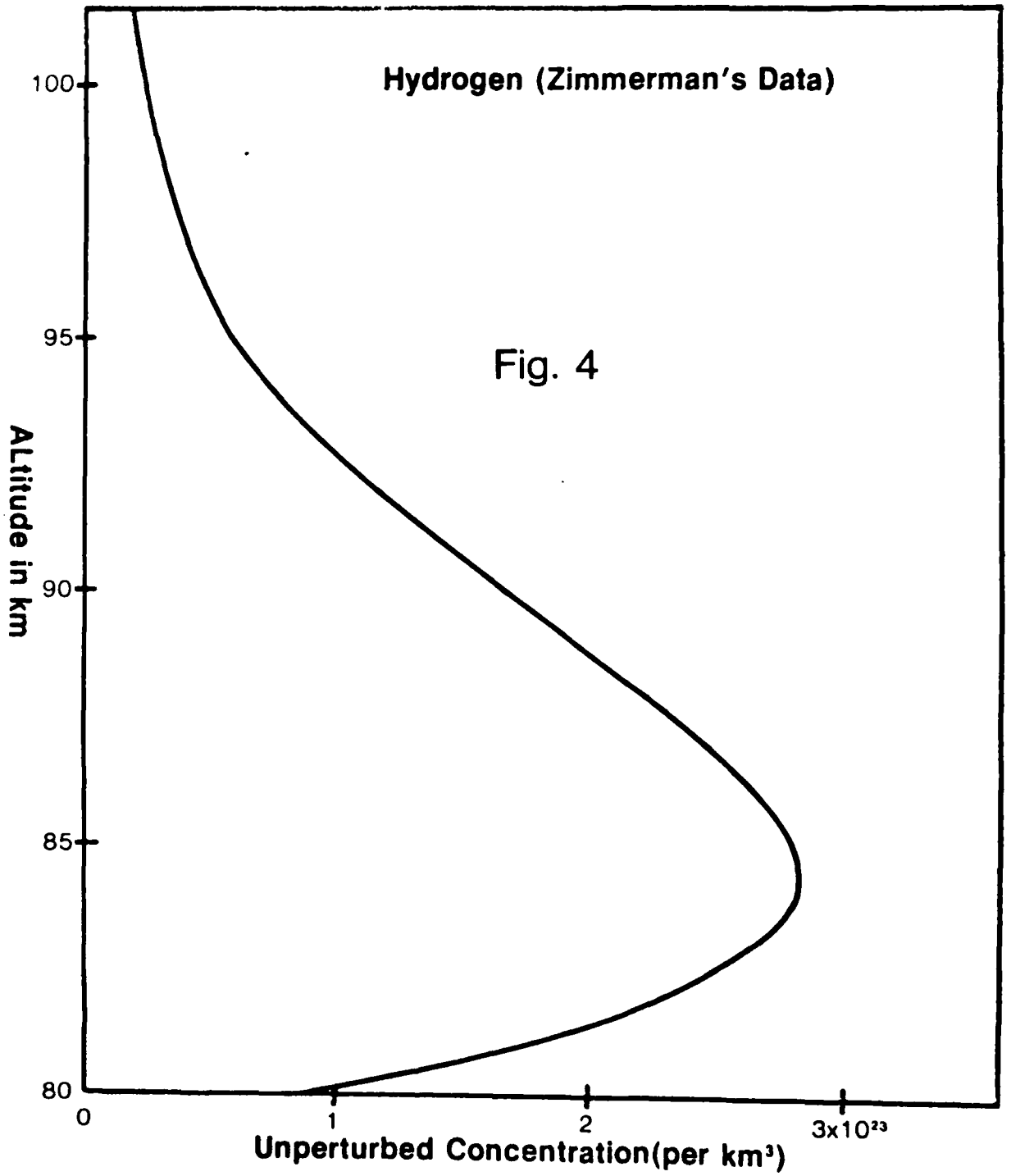
Hydrogen (Zimmerman's Data)
100
95
90
85
80
ALtitude in km
0
1
2
3x10²³
Unperturbed Concentration(per km³)

Fig. 4

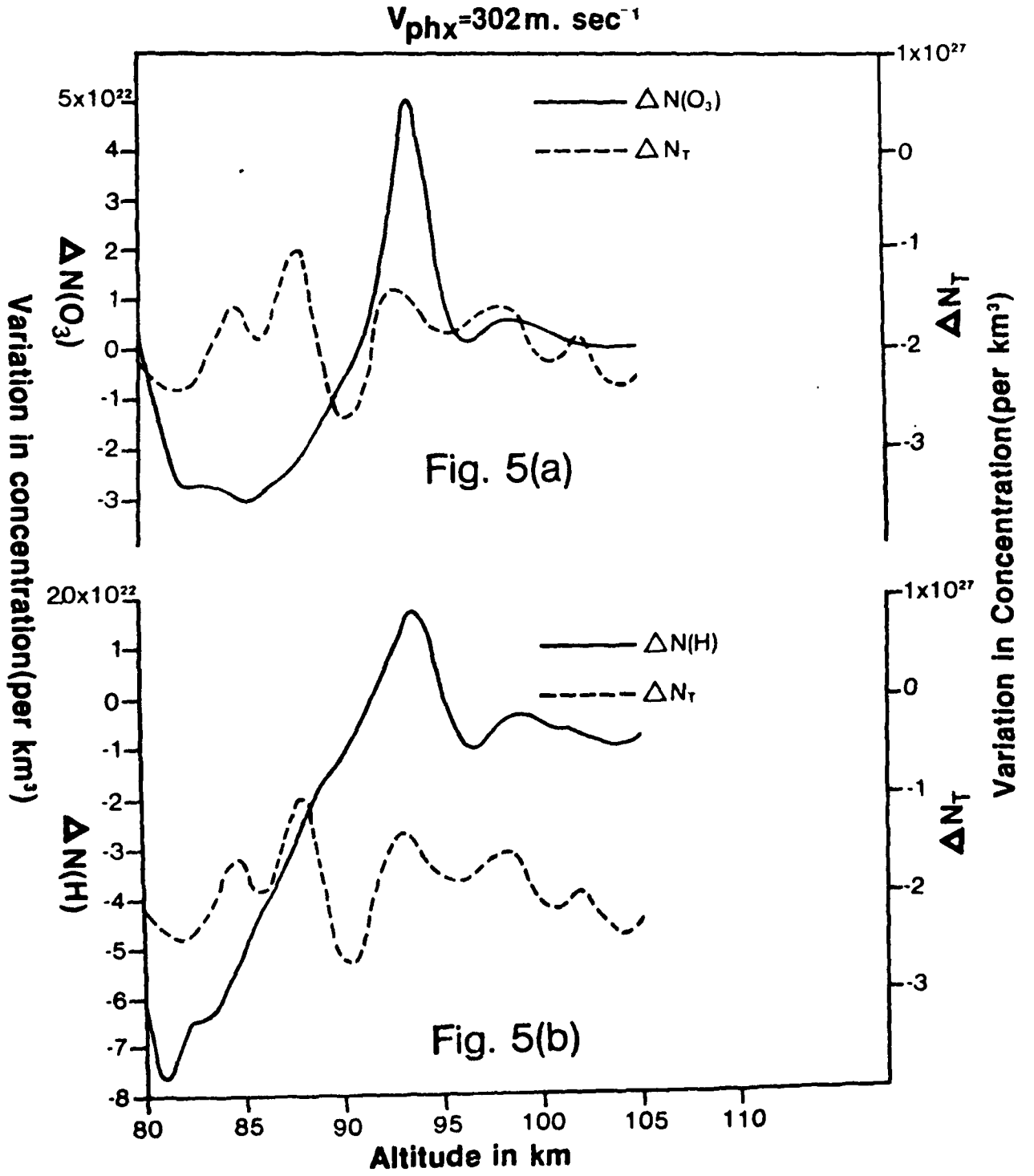
V_{phx}=302m. sec^{-1}
5x10^{22}
4
3
2
1
0
-1
-2
-3
1x10^{27}
0
-1
-2
-3
$\Delta N(O_3)$
ΔN_T
Variation in concentration(per km^3)
Variation in Concentration(per km^3)
Fig. 5(a)
20x10^{22}
1
0
-1
-2
-3
-4
-5
-6
-7
-8
1x10^{27}
0
-1
-2
-3
$\Delta N(H)$
ΔN_T
80
85
90
95
100
105
110
Altitude in km
Fig. 5(b)

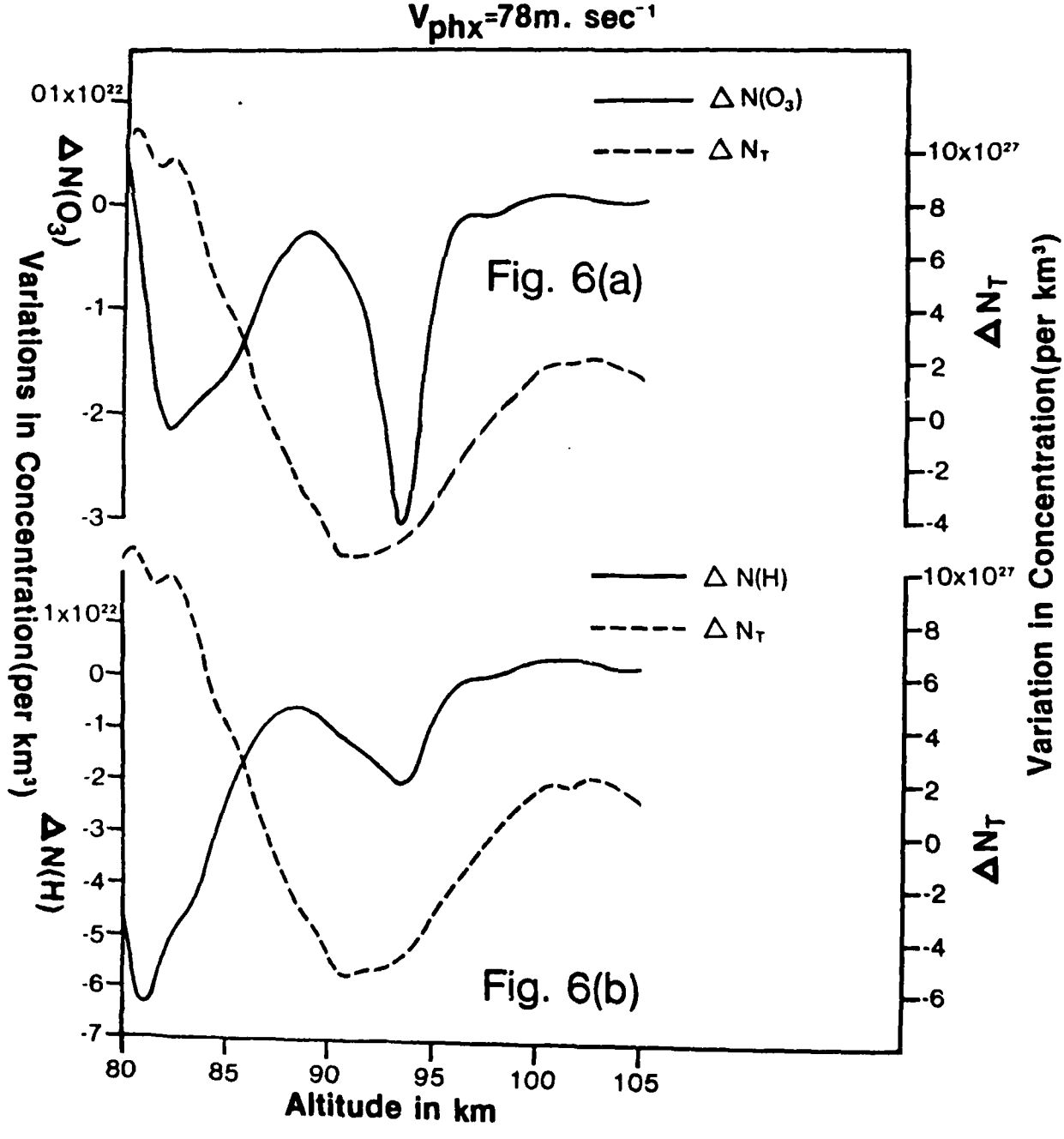
V_{phx}=78m. sec^{-1}
01x10^{22}
$\Delta N(O_3)$
ΔN_T
10x10^{27}
Fig. 6(a)
$\Delta N(O_3)$
ΔN_T
$\Delta N(H)$
ΔN_T
1x10^{22}
10x10^{27}
Fig. 6(b)
Variations in Concentration(per km^3)
Variation in Concentration(per km^3)
80
85
90
95
100
105
Altitude in km

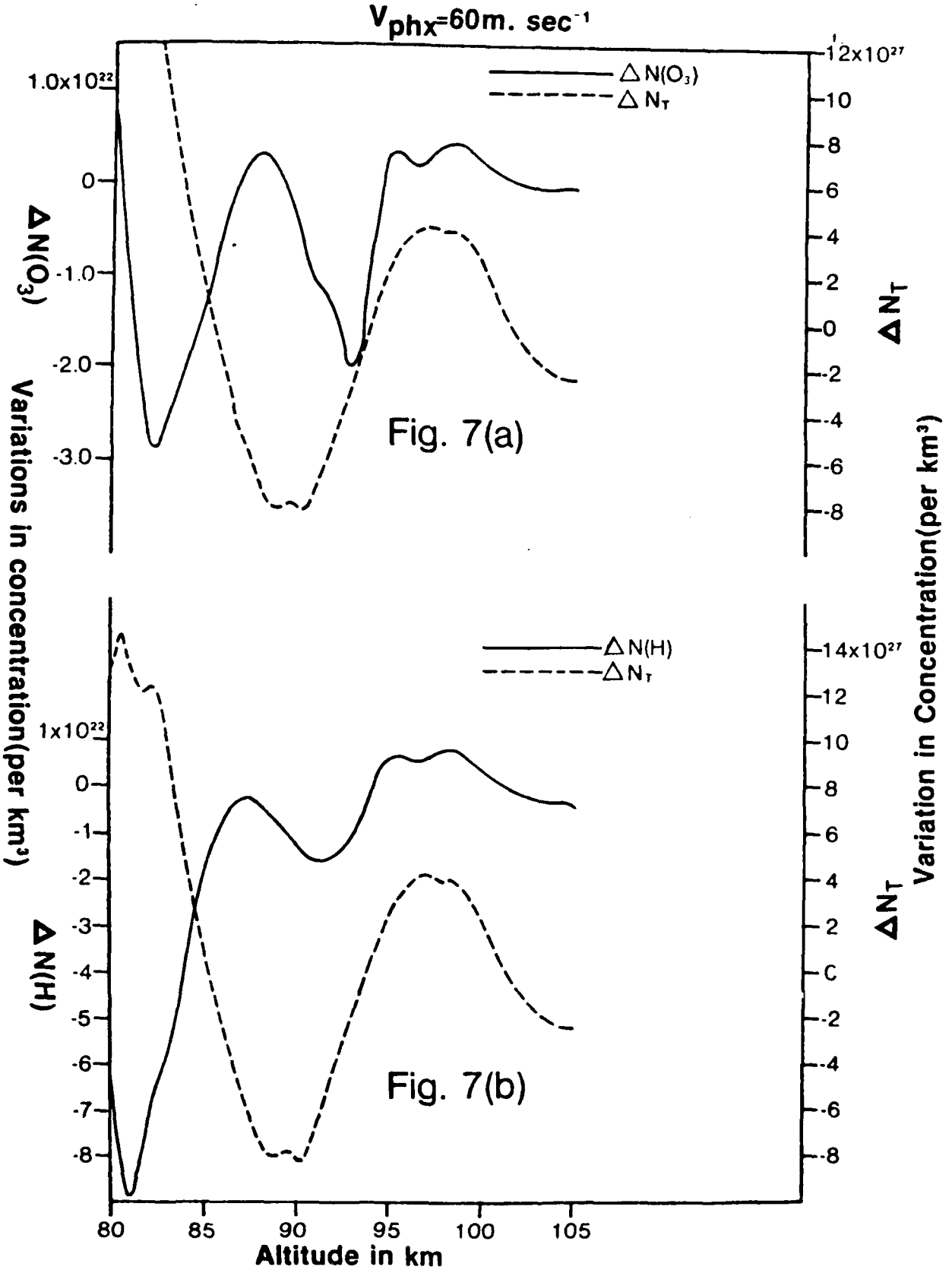
V_{phx}=60m. sec^{-1}
$\Delta N(O_3)$
ΔN_T
1.0x10^{22}
0
-1.0
-2.0
-3.0
$\Delta N(O_3)$
Variations in concentration(per km^3)
12x10^{27}
10
8
6
4
2
0
-2
-4
-6
-8
ΔN_T
Variation in Concentration(per km^3)
Fig. 7(a)
$\Delta N(H)$
ΔN_T
1x10^{22}
0
-1
-2
-3
-4
-5
-6
-7
-8
$\Delta N(H)$
14x10^{27}
12
10
8
6
4
2
0
-2
-4
-6
-8
ΔN_T
Fig. 7(b)
80
85
90
95
100
105
Altitude in km

V_{phx}=33m. sec^{-1}

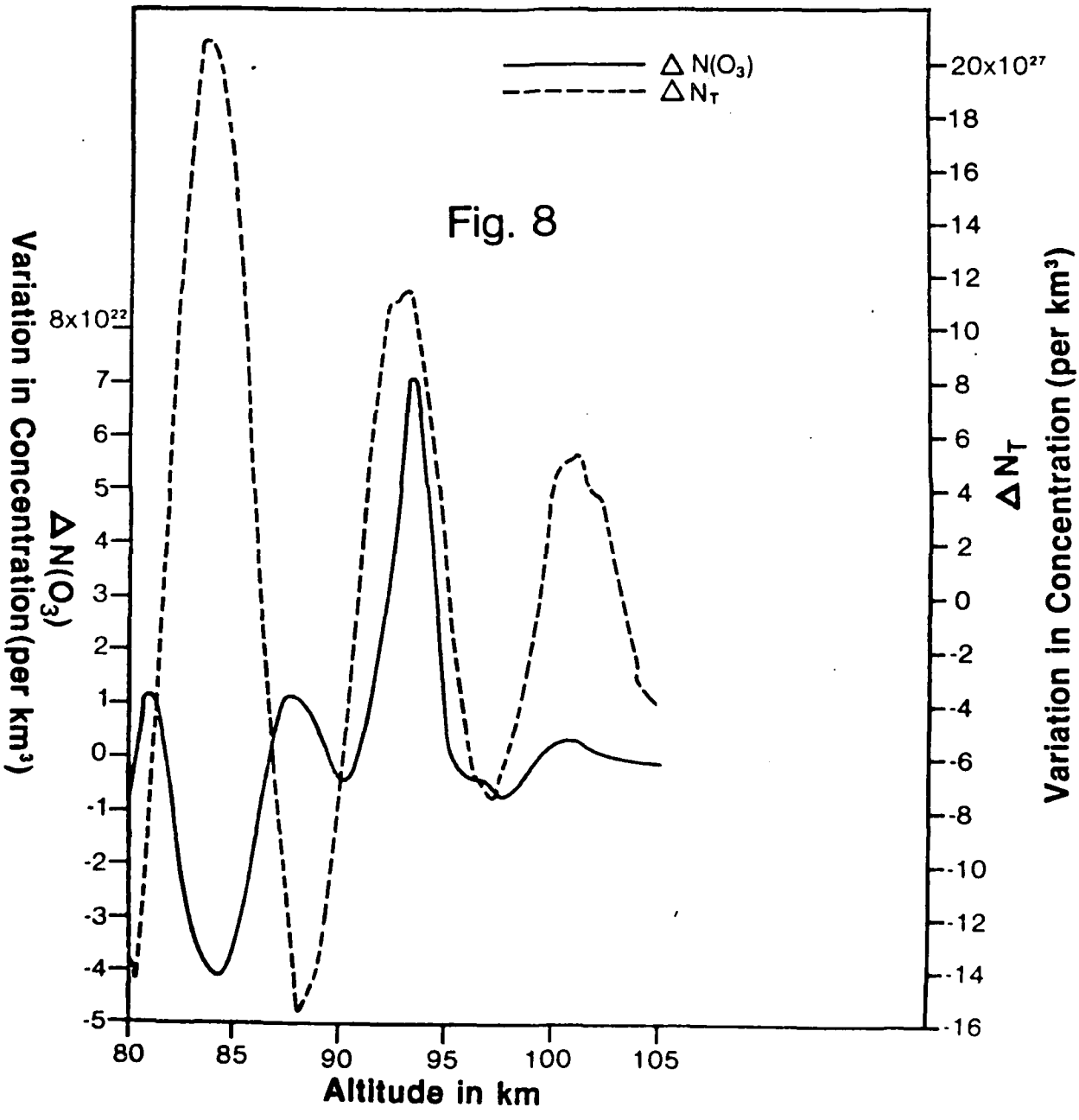

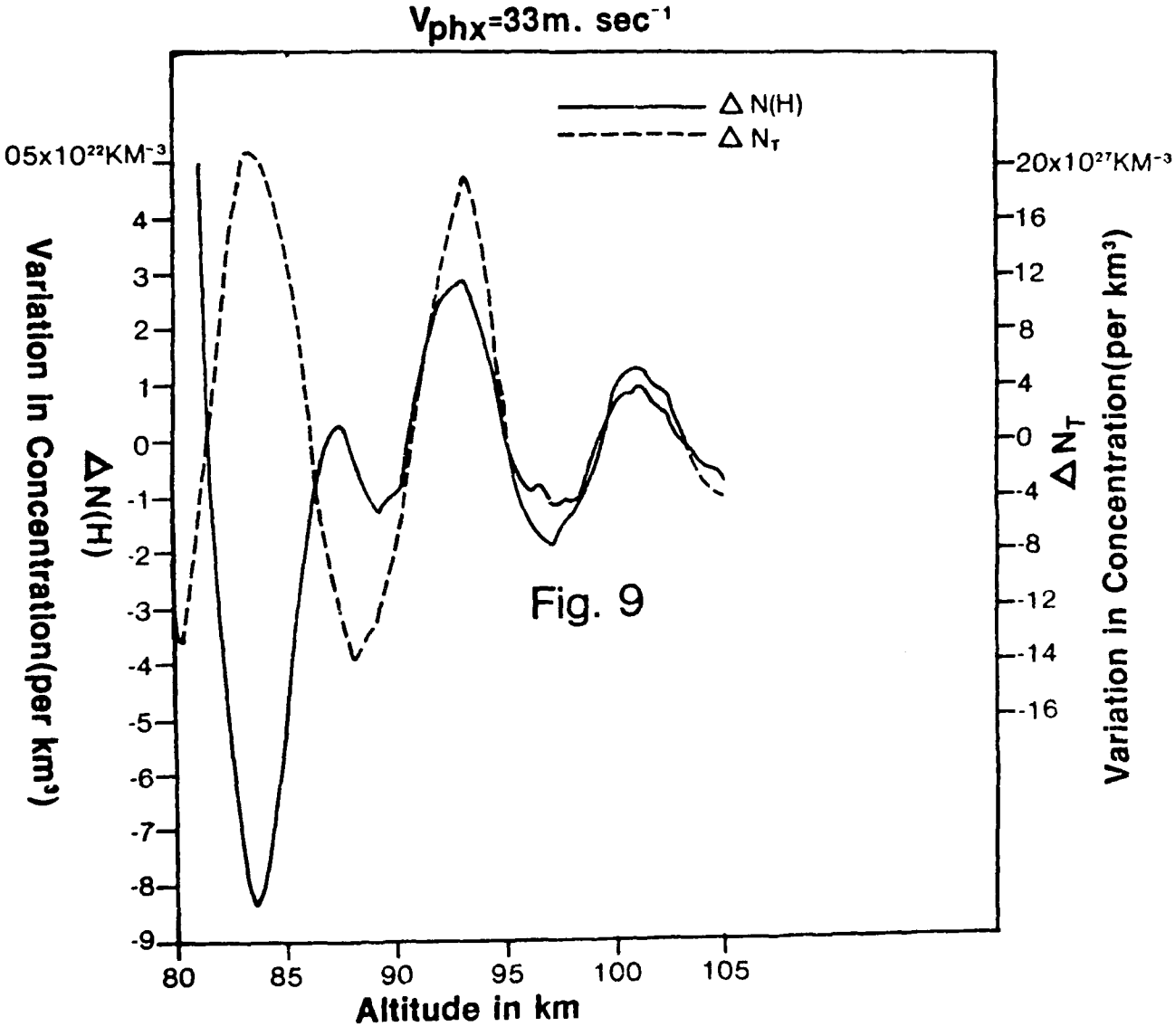
V_{phx}=33m. sec^{-1}
Δ N(H)
Δ N_T
05x10^{22}KM^{-3}
20x10^{27}KM^{-3}
Variation in Concentration(per km^3)
Δ N(H)
Δ N_T
Variation in Concentration(per km^3)
4
3
2
1
0
-1
-2
-3
-4
-5
-6
-7
-8
-9
16
12
8
4
0
-4
-8
-12
-14
-16
80
85
90
95
100
105
Altitude in km

Fig. 9

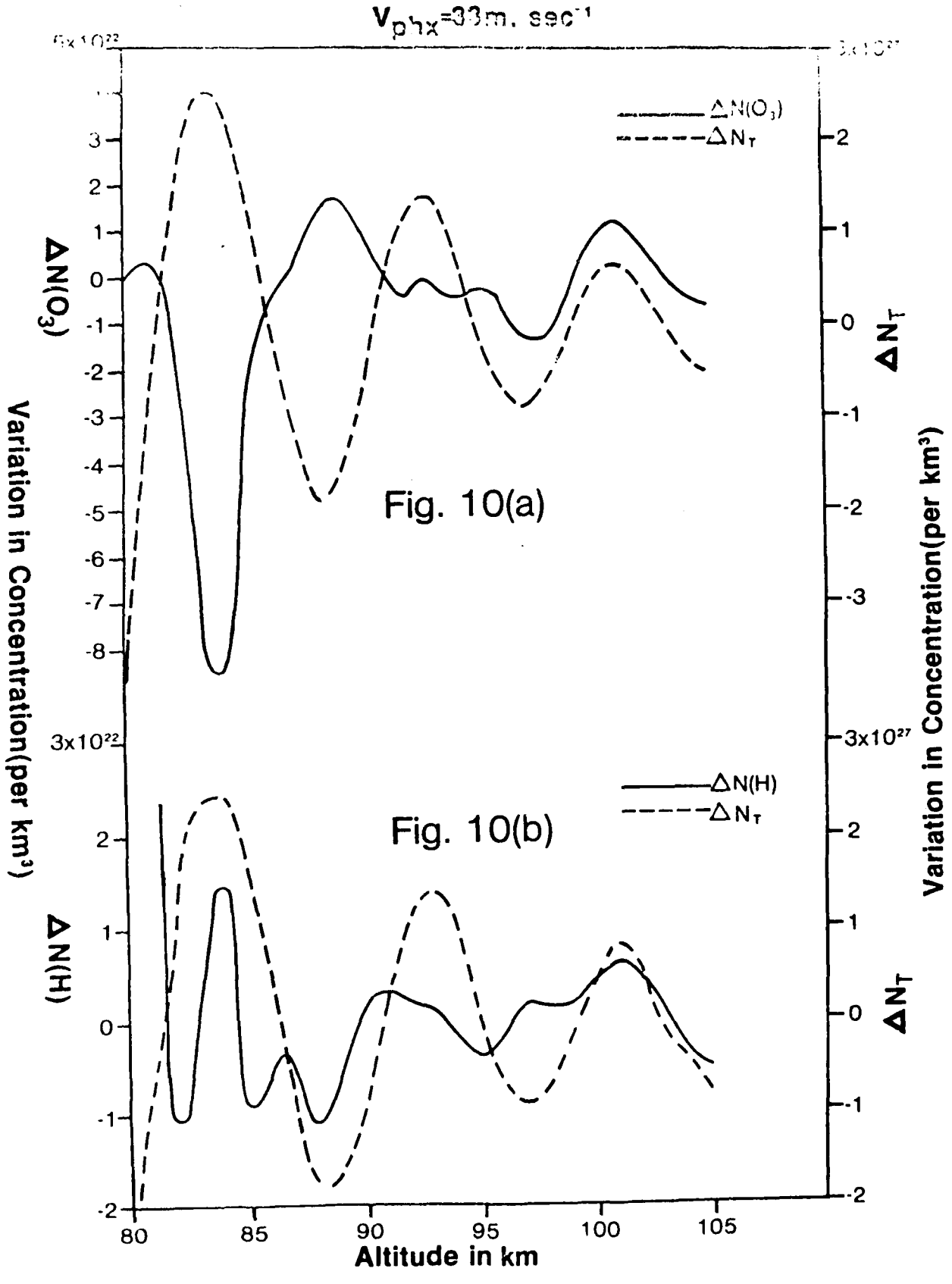
V_{phx}=33m. sec^{-1}
$\Delta N(O_3)$
ΔN_T
$\Delta N(O_3)$
ΔN_T
Variation in Concentration(per km^3)
Variation in Concentration(per km^3)
Fig. 10(a)
$\Delta N(H)$
ΔN_T
Fig. 10(b)
$\Delta N(H)$
ΔN_T
3x10^{22}
3x10^{27}
80
85
90
95
100
105
Altitude in km

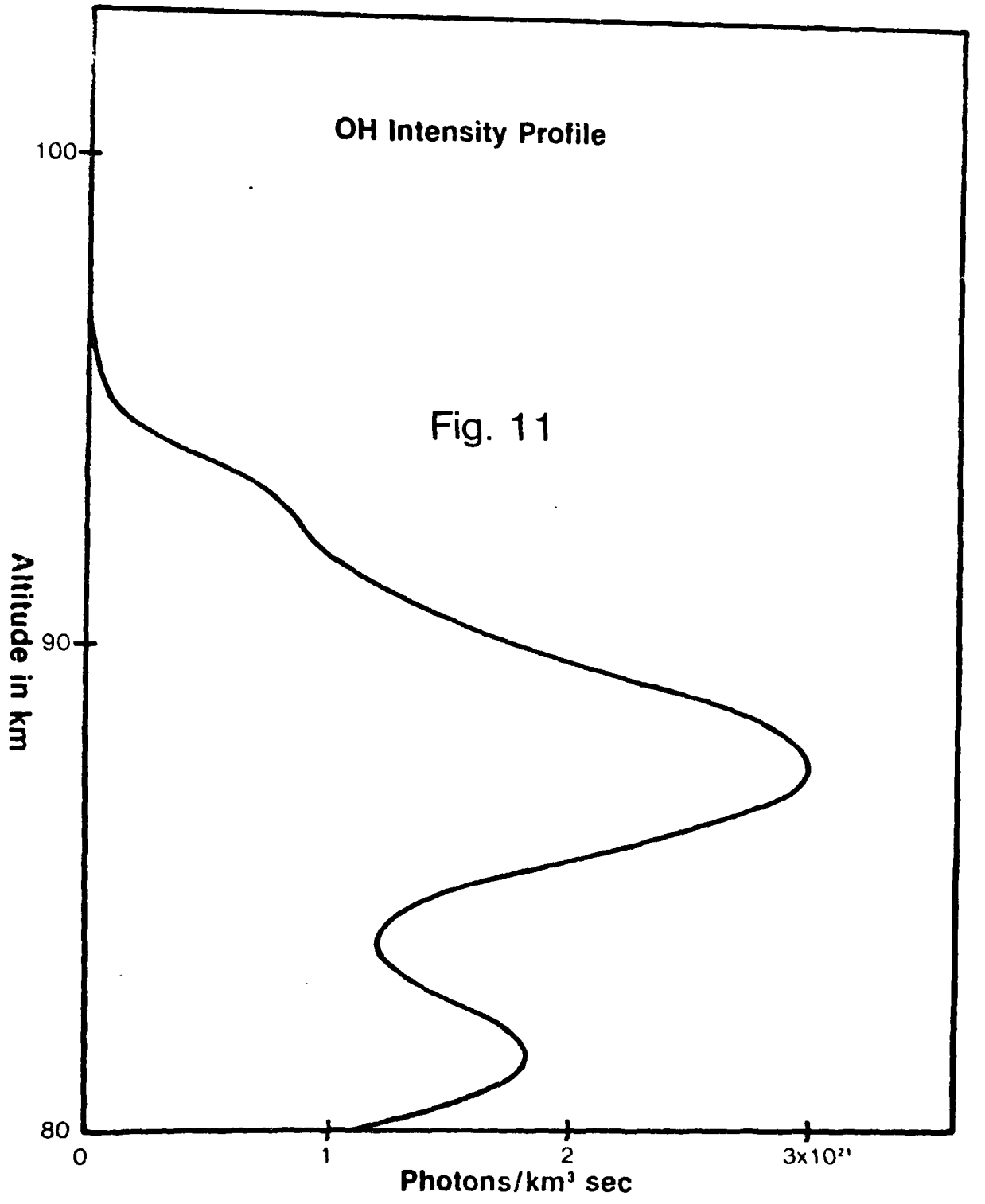
OH Intensity Profile
100
90
80
Altitude in km
0
1
2
3x10²¹
Photons/km³ sec

Fig. 11

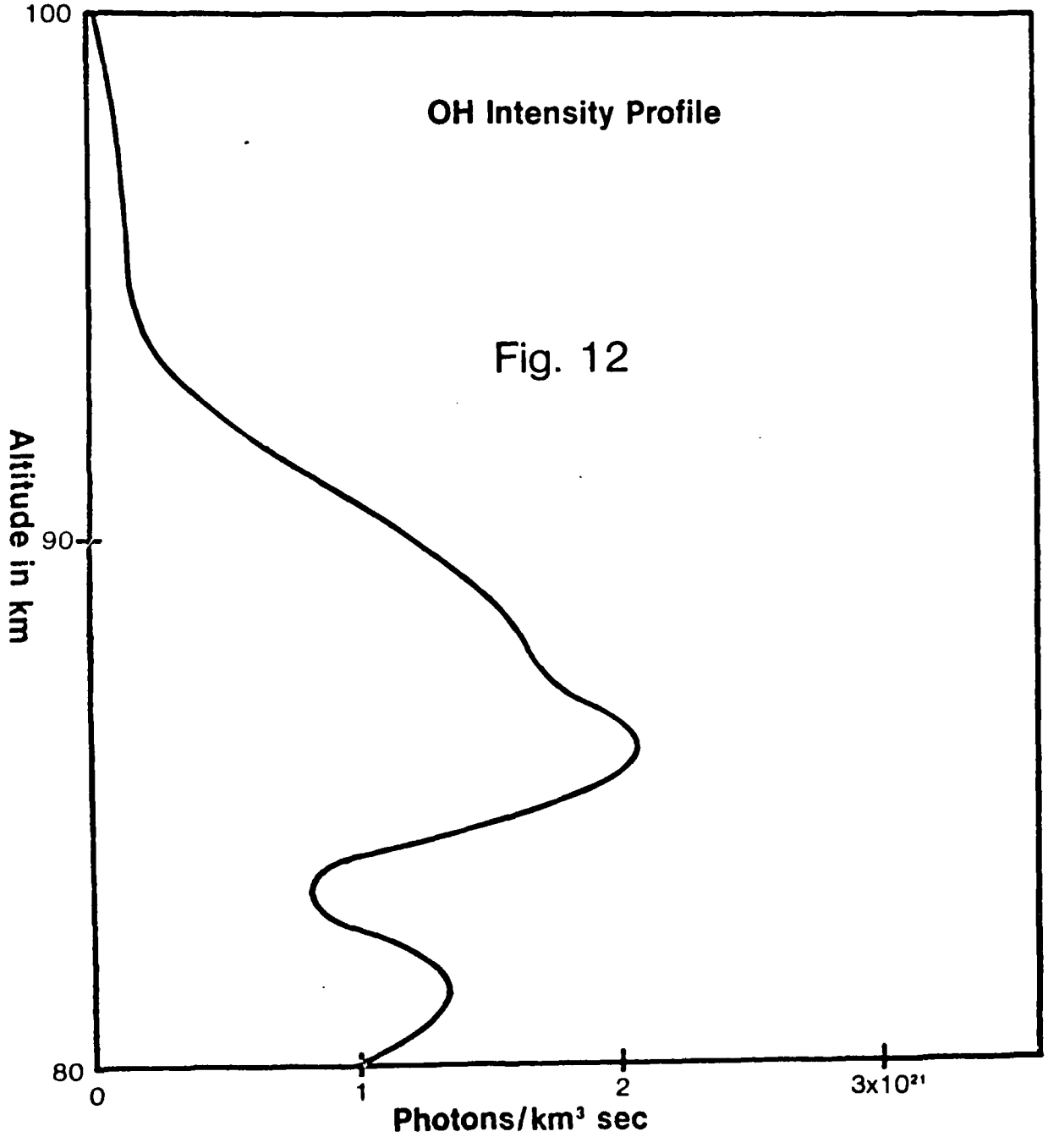
OH Intensity Profile
100
90
80
Altitude in km
0
1
2
3x10²¹
Photons/km³ sec

Fig. 12